FINAL TECHNICAL REPORT

NEHRP/USGS AWARD NUMBER 07HQGR0026

Earthquake Physics, Element III

January 2007 - December 2007

Earthquake Occurrence in Geometrically Complex Systems

Principal Investigator: James Dieterich

University of California, Riverside

Department of Earth Sciences

1230 Geology Building

Riverside, CA 92521

Tel: 951-827-2976

Fax: 951-827-2976

Email: dieterichj@ucr.edu

ABSTRACT

Current standard methodologies for assessing earthquake probabilities are based on models of regional seismicity that employ generic probability distributions for earthquake occurrence and simplified approximations of the physical processes, constitutive properties, and interactions that control the onset of and extent of earthquake slip. One avenue for improving assessment methods, and reducing the large uncertainties in current assessments, is to incorporate more accurate, and region-specific, characterizations of the interactions and physical processes that control earthquake occurrence in fault systems. This project developed and employed an efficient quasi-dynamic earthquake simulator to investigate earthquake occurrence in fault systems including processes that control time, place and extent of earthquake slip. The simulations incorporate rate- and state-dependent fault constitutive properties, which enables modeling of spatial and temporal clustering of earthquakes including foreshocks and aftershocks. Our results indicate that it may be feasible to use fault system simulations to generate site-specific probability density distributions for use in estimating conditional earthquake probabilities.

Background

The physical processes governing the occurrence of earthquakes in fault systems are undoubtedly complex, varied, and poorly understood. Research into those governing processes represents a major scientific challenge in earthquake science because our current inadequate state of knowledge limits our predictive abilities to extrapolate empirical characterizations of seismicity to conditions where observations are sparse (including large earthquake magnitudes, short observation intervals, and possible variability between narrowly defined geographic regions). And it restricts interpretations of seismological observations in terms of material parameters and physical conditions. This project focused on the behavior of fault systems particularly the physical parameters, processes, and interactions that control the space/time characteristics of earthquakes.

The project employed a physics-based 3D earthquake simulator to a) investigate the processes controlling fault slip and earthquake occurrence in geometrically complex fault systems, and b) investigate methods for using physics-based earthquake simulators in regional assessments of earthquake probabilities. The model generates long sequences of earthquakes (>10^5 events) over a wide range of magnitudes (M4.0-M8). Foreshocks and aftershock processes are modeled using solutions for earthquake nucleation with rate- and state-dependent friction.

Modeling approach

For this project we have implemented a highly efficient computational approach developed and tested by Dieterich [1995]. Tests described below indicate the calculations are quite accurate.

The computer code is based on a boundary element formulation whereby interactions among the fault elements are represented by an array of 3D elastic dislocations, and Coulomb stress on the elements in the direction of slip on an element is

$$S_i = K_{ij}\delta_j + S_{L_i}\ ,\ i,j = 1,2,...n \qquad (1)$$

where K_{ij} is an interaction matrix derived from the elastic dislocation solutions, δ_j is slip of fault element j, S_{L_i} is the externally applied (tectonic) stressing at fault element i, and n is the total number of elements (summation convention applies to repeated indices). The code uses the full 3D boundary element representations and it can employ rectangular or triangular fault elements. The model employs rate-state constitutive properties [Dieterich, 1981; Ruina,1983; Rice, 1983] with full coupling of normal stress to fault strength through the coefficient of friction and the friction state-variable θ, which evolves with time, slip and changes of normal stress as given by Linker and Dieterich [1992].

The central feature of the method is the use of event-driven computational steps as opposed to time stepping at closely spaced intervals. The cycle of stress accumulation and earthquake slip at each fault segment is separated into three distinct phases designated as sliding states 0, 1, and 2. A fault element is at state 0 if stress is below the steady-state friction, as defined by rate- and state-dependent friction. In the model this condition is approximated as a fully locked element in which the fault strengthens as the frictional state-variable θ increases with time, *e.g.* $\theta = \theta_0 + t$ at constant normal stress, but modified by effects arising from normal stress changes. The transition to sliding state 1 occurs when the stress exceeds the steady-state friction. During state 1, conditions have not yet been met for unstable slip, but the fault progressively weakens.

Macroscopic slip is negligible. Analytic solutions for nucleation of unstable slip [Dieterich, 1992] generalized for varying normal stress [Dieterich, 2007; Richards-Dinger and Dieterich, in preparation], together with stressing rate determine the transition time to state 2, which is earthquake slip. At tectonic stressing rates earthquake nucleation typically requires a year or more, but during earthquake slip the high stressing rates at the rupture front compress the duration of state 1 to a fraction of a second.

During earthquake slip, the method employs a quasi-dynamical representation that approximates the gross dynamics of the earthquake source. Slip speed during an earthquake (state 2) is set at a constant value using the relationship for elastic shear impedance together with the local dynamic driving stress

$$\dot{\delta}_{EQ_j} = \frac{2\beta\Delta\tau_j}{G}\ , \qquad (2)$$

where the driving stress $\Delta\tau_j$ is the difference between the stress at the initiation of slip and the sliding friction at element j, β is the shear wave speed, and G is the shear modulus. The use of (2) provides a quasi-dynamical representation of time-scales and slip rates for the earthquake event simulations. Some characteristics of the rupture dynamics, and comparisons of single-event rupture simulations with fully dynamical simulations in 3D are discussed below. An element ceases to slip and reverts to state 0 when the stress decreases to some specified stress determined by the sliding friction (with inertial overshoot of stress to levels less than the sliding friction as an adjustable model parameter).

Computational efficiency is obtained from the use of event-driven computational steps, use of analytic nucleation solutions, and specification of earthquake slip speed from the shear impedance relation. Note that change of stressing rate at any element i in response to initiation or termination of earthquake slip at element j is simply

$$\Delta\dot{S}_i = \pm K_{ij}\dot{\delta}_{EQ_j} \quad \text{(no summation)}. \qquad (3)$$

Hence, $1 \rightarrow 2$, or $2 \rightarrow 0$ state transition events require only one multiply and add operation at each element to update stressing rates everywhere in the model (no system-scale updates are required for the $0 \rightarrow 1$ transition). Because the transition times depend only on initial conditions and stressing rates, computations proceed in steps that mark the transition from one sliding state to the next without calculation of intermediate steps. This approach completely avoids computationally intensive solutions of systems of equations at closely spaced time intervals. Computation time for an earthquake event of some fixed size, embedded in a model with n fault elements, scales approximately by n^1.

Results

During the period of the project the model code was thoroughly exercised and, in order to run large models, converted to 64-bit. Additionally, steps were taken towards optimization of the code. It has successfully generated test seismicity catalogs in models with up to 16,000 elements. A Southern California model described below (which contains 4,712 fault elements) takes approximately 8 hours to simulate 500,000 events M4.6 to M8.0 on a single 2.5 GHz G5 CPU.

The current single-processor code can carry out simulations with up to ~30,000 fault elements. We estimate that with 30,000 fault elements, roughly 100,000 earthquakes (M4-M8) can be simulated in 12-24 hours. The computation speed of the code far outperforms that of any other method we know of.

The simulations produce a range of rupture characteristics that are comparable to those obtained in detailed fully dynamical calculations. In multi-event simulations, which have heterogeneous stresses at the initiation of rupture, rupture propagation speeds are typically 2.0 to 2.4 km/s. In those simulations model parameters were set to give average dynamic stress drops and slip speeds of 5 MPa and 1 m/s respectively, with an implicit shear wave speed of 3 km/sec. Rupture growth and slip in simulations can be crack-like, or consist of a narrow slip-pulse [Heaton, 1990]. Factors favoring crack-like behavior in the simulations are relatively smooth initial stresses and weak healing following termination of slip, while slip-pulse behavior arises with heterogeneous initial stresses and strong fault healing following rupture termination. This behavior is consistent with fully dynamical rupture simulations [Beroza and Mikumo, 1996; Zheng and Rice, 1998]. The strength of fault healing following the termination of slip is controlled by a single adjustable parameter in the code.

As a matter of good scientific practice we have endeavored to be rigorous in testing the simulator at every stage of development. A key performance measure of the rupture simulations is the accuracy with which the simulations predict a) the extent of earthquake rupture given a stress state at the initiation of an earthquake, and b) the slip distribution in that rupture, which determines the details of the stress state in the model following an earthquake (and therefore subsequent earthquake history). Figure 1 shows some comparisons of calculations with the fast simulator and with DYNA3D, a fully dynamic 3D finite element code used by David Oglesby of UC Riverside. The calculations were performed in 2007 by a SCEC summer undergraduate intern, Christine Burrill. Rupture characteristics depend on details of fault constitutive properties. The DYNA3D simulations are based on slip-weakening friction with specified static and sliding friction. Hence, rate-state friction parameters and initial conditions were set to match, as closely as possible, the friction, stress, and rupture conditions in DYNA3D. Under a variety of initial stress conditions, the rupture character (crack-like vs. pulse-like), rupture velocity, and final patterns of stress drop and slip calculated with the rapid simulator agreed remarkably well with DYNA3D.

We investigated methods to implement dynamic stressing in the model. A promising approach is to use the quasi-dynamical simulations as a kinematic source to compute seismograms with the Greens functions for a homogenous elastic whole-space [e.g. Aki and Richards, 2002]. Because analytic solutions for earthquake nucleation can be used to determine if dynamic stresses trigger unstable slip (1→2 state transition) the implementation of dynamic triggering of slip should not be too costly in terms of computational speed. Figure 2 shows test computations for a rupture on a planar fault with uniform initial stress and the corresponding seismogram obtained with DYNA3D, a dynamic 3D finite element simulation code. The DYNA3D amplitudes are a factor of about 2 larger than our results due to our use of whole-space Green's functions. Addition of an image source with the Green's functions will bring the solutions to with about 10-15% of DYNA3D. Figure 3 gives an example of seismograms for a complex rupture with heterogeneous initial stresses inherited from previous events in a long simulation.

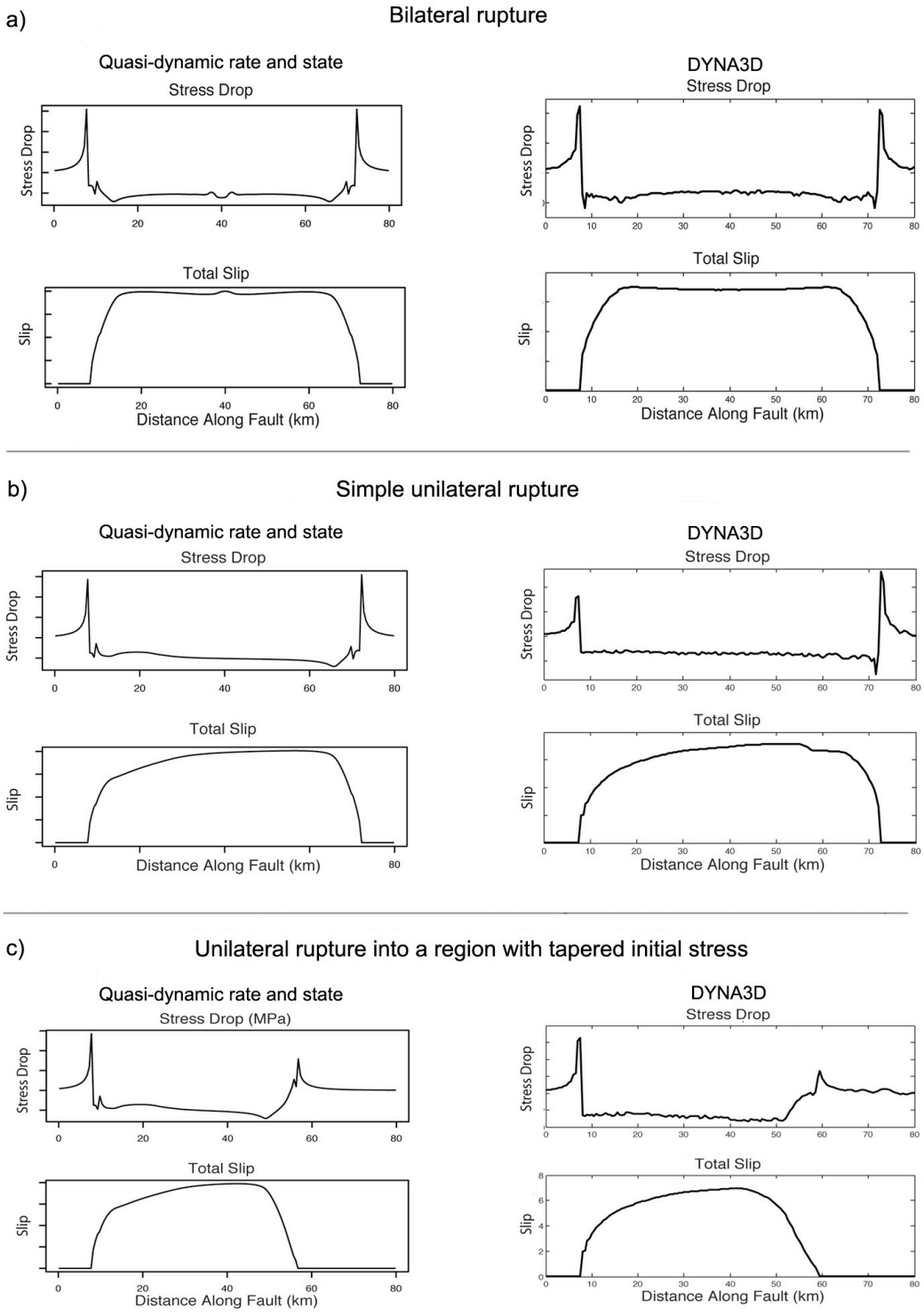

Figure 1. Comparisons of 3D rupture simulations on planar faults with the fast simulator (left) and with DYNA3D, a fully dynamic finite element code [Burrill, Richards-Dinger, Oglesby and Dieterich, in preparation]. a) Bilateral rupture with uniform stress and friction conditions over the entire rupture area (except for the nucleation region). b) simple unilateral rupture with initiation point at left end and with hard rupture limits at ends. c) Unilateral rupture as in b), but with soft boundary at right (tapered stress) that allowed progressive penetration of the rupture.

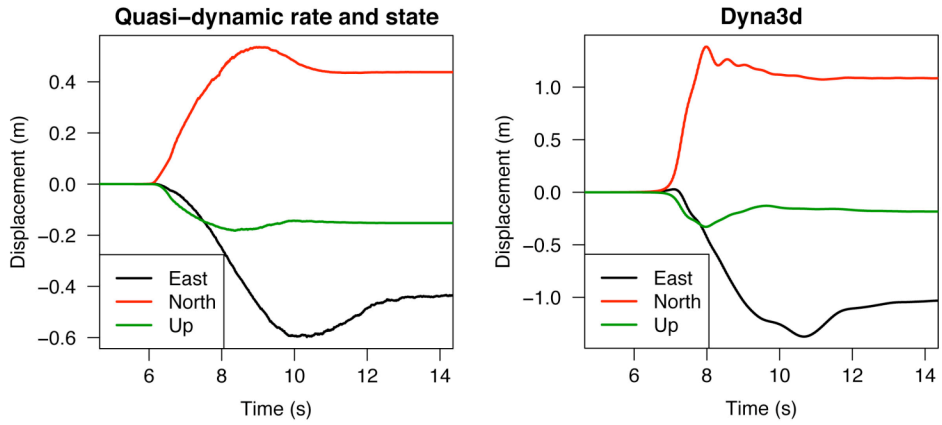

Figure 2. Displacement seismograms produced by a magnitude 7.2 bilateral rupture on a vertical left-lateral, strike-slip fault (64km long by 8km deep) with homogenous initial stress. (right panel) results from DYNA3D. (left panel) results from the slip functions produced by our quasi-dynamic model with Greens functions for a homogenous elastic whole-space. The fault strikes due North. These seismograms are for a surface station 2 km east of the southern end of the fault.

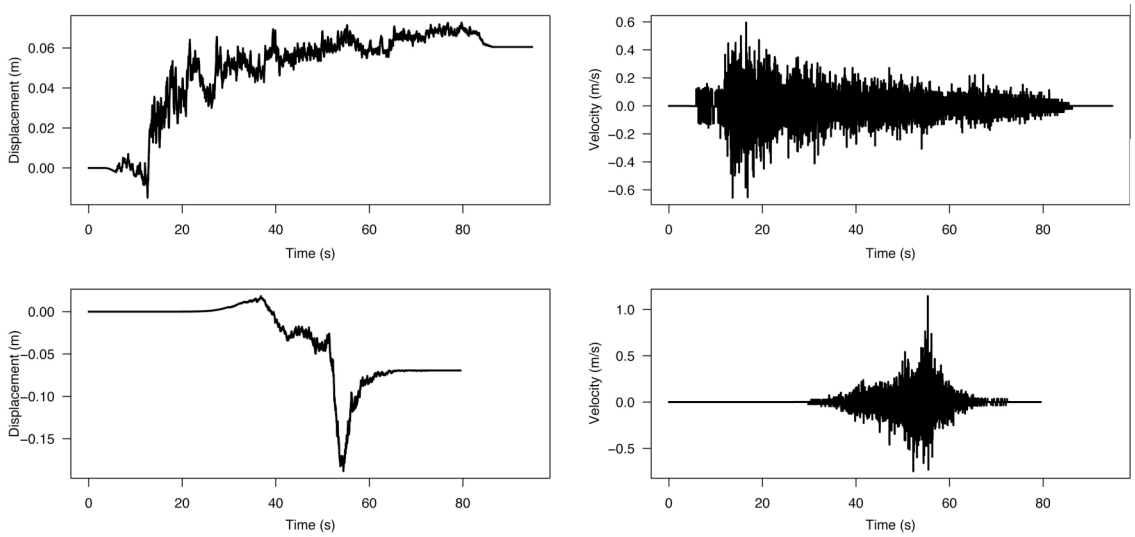

Figure 3. Displacement (left panels) and velocity (right panels) seismograms produced by a complex rupture in our quasi-dynamic model from an event with heterogeneous initial stresses inherited from previous events in a long (50,000 event) simulation. The rupture propagated predominantly from north to south on a vertical strike-slip fault. The upper panels are for a station 10km off the northern end of the fault and the lower panels for one a similar distance off the southern end. There is a strong directivity effect, with the latter waveforms compressed relative to the former.

A core objective of the project was to simulate earthquake interactions in geometrically complex fault systems, wherein shear and normal stress vary simultaneously during slip and couple to state evolution, nucleation and sliding resistance. A simple example of this is simulation of seismicity on fractally rough faults, where shear and normal stress interactions operate at all length scales. Compared to planar fault simulations, the fractal faults are characterized by patchy slip, which is reminiscent of inverse solutions for earthquake sources. In fractal fault simulations,

preliminary tests suggest that smaller earthquakes occur preferentially along releasing bends. Restraining bends fail preferentially in the largest earthquakes.

We find that magnitude frequency statistics in the simple models examined thus far are affected by a number factors including heterogeneity of driving stress, fractal fault geometry and amplitude of roughness, and details of the rupture failure criteria. Alone, frequency-magnitude statistics in the model appear to have limited value in restricting parameter space, though the topic needs to be studied more thoroughly.

The model produces clustered seismicity that includes foreshocks, aftershocks and large event clusters. These features are a consequence of the time- and stress-dependence of the state 1 nucleation. Simulation of foreshocks and aftershocks enables direct comparisons with earthquake catalog data, without declustering, and allows modeling of time-dependent earthquake interaction probabilities. Statistically, the simulated aftershocks decay by $1/t^p$ where p has values in the range 0.5 to 1.0. Previously it was shown that foreshock/mainshock statistics and aftershock productivity in this type of simulation can be adjusted to match catalog statistics though adjustment of the rate-state friction parameter A and normal stress σ [Dieterich, 1995]. Figures 4a and 4b compare clustering statistics from a simulation with a compilation of worldwide seismicity by Kagan and Jackson [1991]. The figures show the rate of occurrence of all possible earthquake pairs, M≥6, by the time intervals separating the pairs for different distance intervals. The differences between simulated and observed catalogs arise principally from incomplete catalog data at short times following large earthquakes and truncation at 1000 days by Kagan and Jackson.

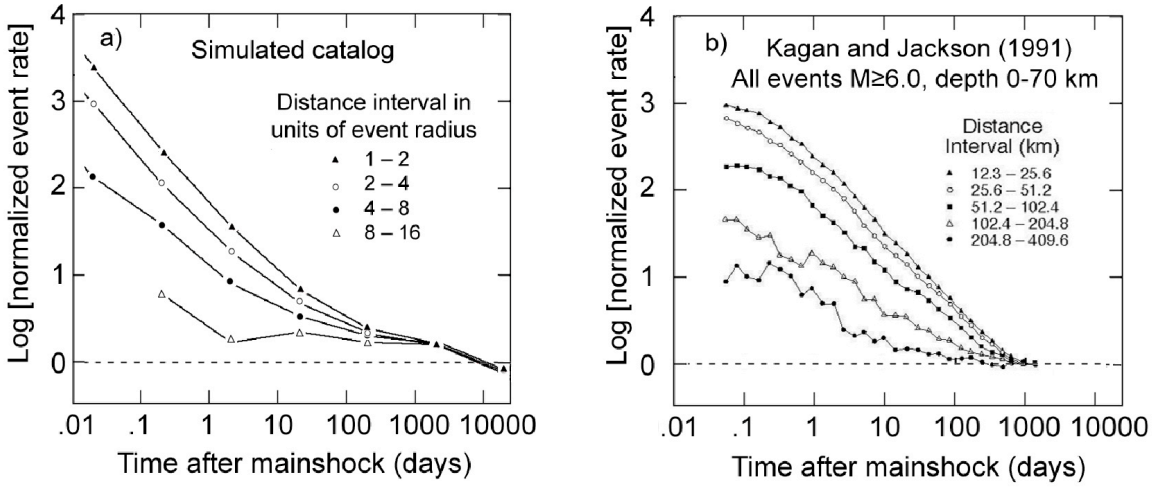

Figure 4. Normalized occurrence rate of all possible earthquake pairs, by the time interval between pairs and separation distance. For purely random occurrence, as described by a Poisson process, the logarithm of the normalized rate = 0 independent of separation distance. Clustering in these plots has Omori-law decay with time, and decay with the separation distance. The principal clustering effect is due to aftershocks with lesser contribution from foreshocks. a) Data from simulated catalog with 50,000 events. B) Harvard catalog data re-plotted for interval distances from Kagan and Jackson [1991].

As an initial experiment with somewhat realistic fault systems where interactions among multiple faults operate, we have constructed a model (Figure 5) that is based on the central and southern San Andreas Fault and major sub-parallel subsidiary faults (San Jacinto and Elsinore). The model consists of eight major segments based on Jennings [1994], with added random

fractal roughness. Each segment was driven at a slip rate based on geodetic measurements and geologic offsets [WGCEP, 1995]. The model contains 4,712 fault elements (each approximately 2 km x 2 km) and the simulation consisted of 500,000 earthquake events. Figure 5 shows a sequence of three large events propagating south along the San Andreas over several months. Most large events do not trigger other large events at such short time intervals; of the 220 events over magnitude 7 in the catalog, 137 were isolated by at least 4 years from the nearest other such event, while there were 34 pairs and 5 triplets that occurred within 4-year intervals.

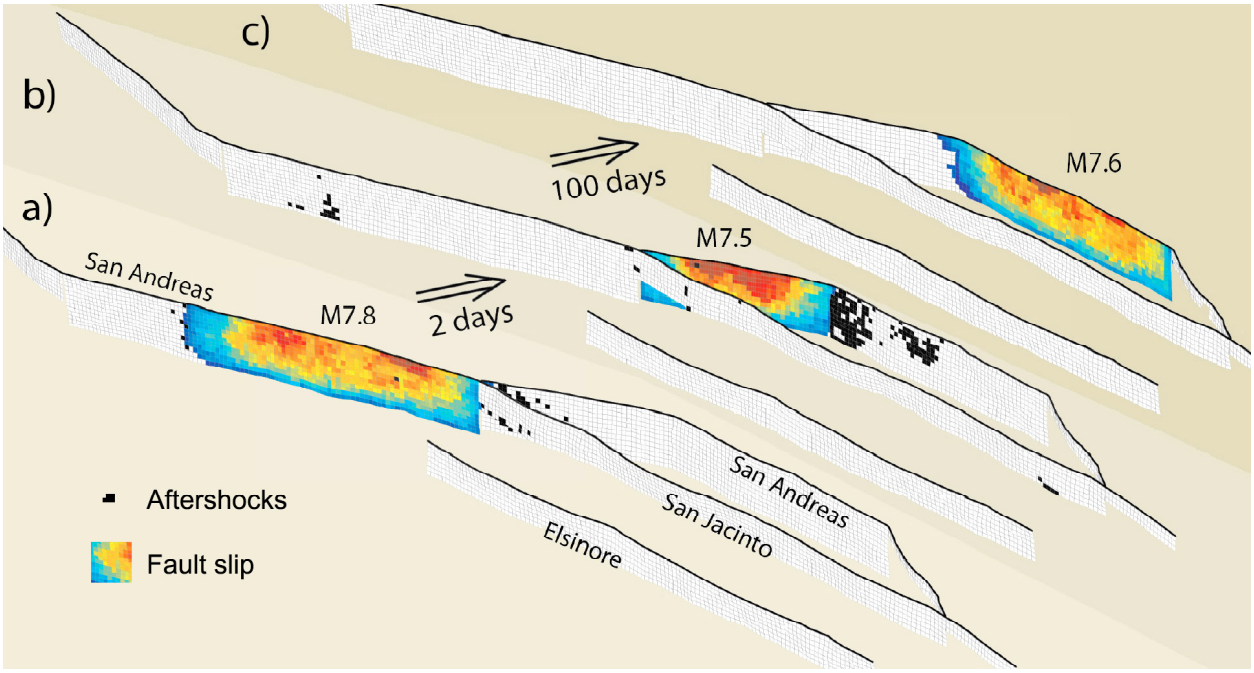

Figure 5. Fault slip (color contours) in a cluster of large events and aftershock hypocenters (black) from a test simulation of the southern San Andreas fault system. In the cluster illustrated here, the Big Bend section of the San Andreas Fault broke in an M7.8 event (panel a) followed by an M7.5 on the San Bernardino section (panel b), and an M7.6 event on the Coachella section (panel c). There were 72 aftershocks in the 2-day interval between the M7.8 and M7.5 events (hypocenters in black in panel a) and 183 aftershocks in the 100-day interval between the M7.5 and M7.6 events (hypocenters in black in panel b). The second and third large events initiated in the regions of high aftershock activity.

Clusters of large events, though relatively uncommon in nature are certainly a well-established characteristic of earthquake occurrence. Clustering of large earthquakes often consists of earthquake pairs [Kagan and Jackson, 1999], but clusters with more numerous events are also seen. A familiar example is the Joshua Tree (1992, M_w 6.1) – Landers (1992, M_w 7.3) – Big Bear (1992, M_w 6.2) – Hector Mine (1998, M_w 7.1) sequence of events in southern California. Other important examples are the series of great earthquakes following the Sumatra mega-earthquake of 2004, and recurring event pairs along the Nankai region of Japan (two M_w 8+ events separated by 32 hours in 1854, and the 1944 M_w 8.2 and 1946 M_w 8.1 pair at similar locations to the 1854 earthquakes). The recurring Nankai pairs are particularly interesting because they suggest that tendency for clustering on a specific section of fault may persist through time.

Current methodologies for assessing time-dependent earthquake probabilities rely on idealized generic probability distributions for earthquake recurrence that are applied globally to all faults for all magnitude ranges. We find that models containing multiple faults and fault segments, in which interactions are important, have earthquake recurrence characteristics that are quite different from isolated faults. Figure 6 shows recurrence statistics as probability density distributions for the next earthquake slip event at a specific point on the fault following a prior earthquake at that point. For reference, the top panel is for a model consisting of a single planar strike-slip fault. The second panel is for two identical, parallel strike-slip faults, and the final panel illustrates recurrence statistics along one segment of the southern California model illustrated in Figure 5. In all cases, the peaks at short recurrence times (0 to 4 years) represent highly clustered activity in the form of foreshocks and aftershocks, where the rupture in the second event wholly or partially re-ruptured the area of slip in the first earthquake. These events have a characteristic t^{-p} fall-off with time. Note the decrease in the foreshock/aftershock peak with increasing magnitude. In the single-fault model, the larger, characteristic events are highly periodic. However, just the addition of a second, identical fault parallel to the first has a profound effect on the recurrence statistics of the large events, with multiple peaks in the pdf and a much less periodic nature (an order of magnitude less as measured by the coefficient of variation).

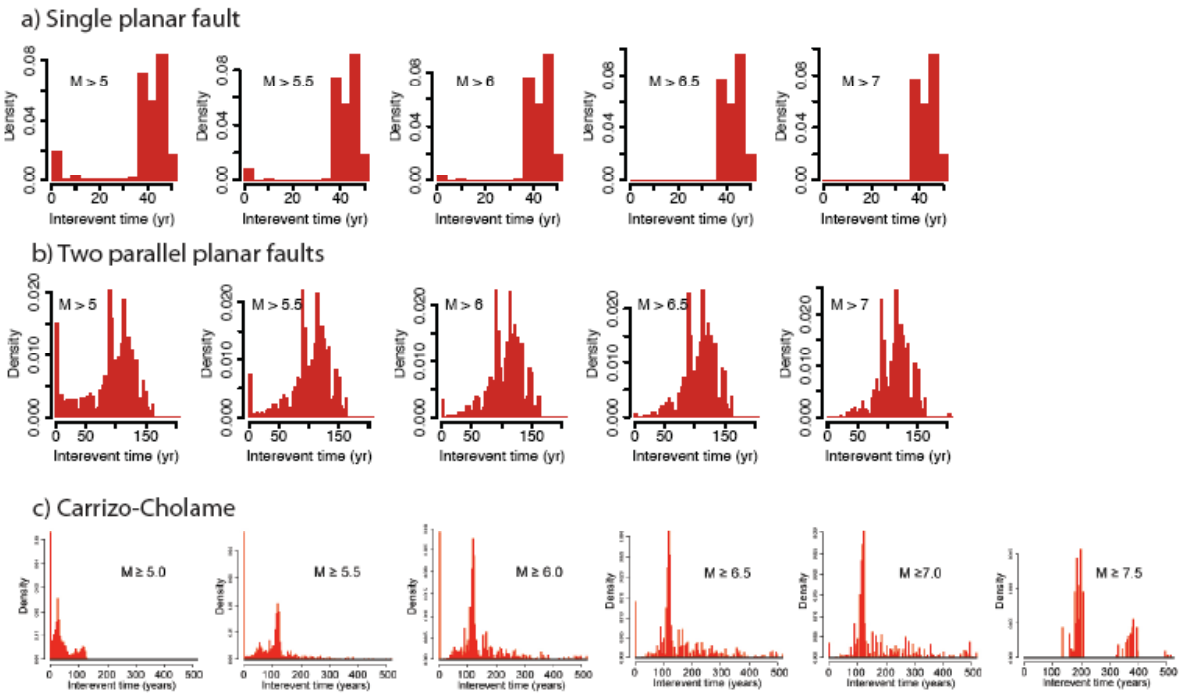

Figure 6. Recurrence statistics for several models presented as probability density functions (pdfs) for the next earthquake slip event at a specific point on the fault following a prior earthquake at that point. The plots are constructed by taking the sum of the individual pdfs at each point on the fault for the magnitude range indicated.

The lower panel of Figure 6 shows the recurrence statistics for one of the eight segments in the southern California model in a synthetic catalog of 500,000 events M4.6 to M8.0. The pdfs are quite complex, vary strongly with magnitude and from segment to segment, and are not easily represented by any analytic functional form. Note especially the growth of long recurrence

interval outliers with increasing magnitude and abrupt shift in the peak at ~120 years for M>7.0, to ~190 years for M>7.5. We note that the recurrence statistics do no bear a resemblance to any any idealized pdf, However, as found in earthquake catalogs, the simulations show combined characteristics of Poisson, clustered, and quasi-periodic recurrence. Indeed the shapes of the curves vary from one fault section to the next suggesting local fault geometry plays an important role setting the characteristic of earthquake recurrence. Additionally, the distributions show a clear magnitude dependence, which is not considered in current methodologies.

References

Aki, K., and P. G. Richards, Quantitative Seismology, 2nd Ed., University Science Books, 2002.

Beroza, G. C., and T. Mikumo, Short slip duration in dynamic rupture in the presence of heterogeneous fault properties, J. Geophys. Res., 101, 22,449–22,460, 1996.

Dieterich, J., Constitutive properties of faults with simulated gouge, in Monograph 24, Mechanical Behavior of Crustal Rocks, edited by N. L. Carter, M. Friedman, J. M. Logan, and D. W. Sterns, pp. 103–120, American Geophysical Union, Washington, D.C., 1981.

Dieterich, J. H., Earthquake nucleation on faults with rate- and state-dependent strength, Tectonophysics, 211, 115–134, 1992.

Dieterich, J. H., Earthquake simulations with time-dependent nucleation and long-range interactions, Journal of Nonlinear Processes in Geophysics, 2, 109–120, 1995.

Dieterich, J., Applications of rate-and-state-dependent friction to models of fault slip and earthquake occurrence, in Treatise On Geophysics, Vol. 4, edited by G. Schubert, Elsevier, Oxford, 2007.

Heaton, T. H., Evidence for and implications of self-healing pulses of slip in earthquake rupture, Phys. Earth Planet. Inter., 64, 1–20, 1990.

Jennings, C.W., Fault activity map of California and adjacent areas with locations and ages of recent volcanic eruptions, Calif. Div. of Mines and Geol., Dep. of Conserv., Sacramento, 1994.

Kagan, Y. Y., and D. D. Jackson, Long-term earthquake clustering, Geophys. J. Int., 104, 117–134, 1991.

Kagan, Y. Y., and D. D. Jackson, Worldwidw Doublets of Large Shallow Earthquakes, Bull. Seismol. Soc. Am., 89, 1147-1155, 1999.

Linker, M. F., and J. H. Dieterich, Effects of variable normal stress on rock friction - Observations and constitutive equations, J. Geophys. Res., 97, 4923–4940, 1992.

Rice, J. R., Constitutive relations for fault slip and earthquake instabilities, Pure and Applied Geophysics, 121, 443–475, 1983.

Ruina, A., Slip instability and state variable friction laws, J. Geophys. Res., 88, 10,359–10,370, 1983.

Working Group on California Earthquake Probabilities (WGCEP), Seismic hazards in southern California: Probable earthquakes, 1994-2024, Bull. Seismol. Soc. Am., 85 , 379–439, 1995.

Zheng, G., and J. R. Rice, Conditions under which velocity-weakening friction allows a self-healing versus a cracklike mode of rupture, Bull. Seismol. Soc. Am., 86 , 1466–1483, 1998.